THE EFFECT OF COOLING RATE ON STRUCTURE AND CORROSION RESISTANCE OF $Fe_5CrCuNiMnSi$ AND $Fe_5CoCuNiMnSi$ HIGH-ENTROPY ALLOYS

O.I. Kushnerov*, V.F. Bashev. V.A. Polonskyy

Oles Honchar Dnipro National University, Dnipro, Ukraine
e-mail: kushnrv@gmail.com

The structure, phase composition, electrochemical behavior, and corrosion resistance of high-entropy alloys $Fe_5CrCuNiMnSi$ and $Fe_5CoCuNiMnSi$ in as-cast and splat-quenched states were studied. A cooling rate estimated by splat-quenched film thickness was ~ 10^6 K/s. Selecting the components of the studied alloys was carried out basing on the criteria adopted in the literature for the composition of a high-entropy alloy such as calculations of the entropy and enthalpy of mixing, valence electron concentrations as well as the difference between the atomic radii of the components. Using X-ray diffraction analysis, the phase composition and crystal lattice parameters of the investigated high-entropy alloys were determined. It was established that the as-cast $Fe_5CoCuNiMnSi$ alloy is a solid solution with a face-centered cubic lattice, while the as-cast $Fe_5CrCuNiMnSi$ alloy contains two solid solutions with a face-centered and solid solution with body-centered cubic lattices. However, both spalt-quenched high-entropy alloys were solid solutions with a face-centered cubic lattice. The values of stationary potentials and areas of electrochemical stability of alloys as well as the density of corrosion currents were determined. It was shown that samples of the Fe5CrCuNiMnSi alloy behaved inertly in corrosion tests both in as-cast and in splat-quenched states.

Keywords: high entropy alloy, structure, phase composition, splat-quenching, microhardness, corrosion resistance.

Received 06.11.2021; Received in revised form 09.12.2021; Accepted 10.12.2021

1. Introduction

Until recently, it was believed that the creation of alloys was possible only if you choose one component as a basis (alloys based on Fe, Cu, Al, Ni, Mg, etc.). However, these claims were dispelled after obtaining the so-called high-entropy alloys (HEAs) consisting of five or more components in equal equimolar ratios. With certain combinations of elements in these alloys, it is possible to obtain high strength, ductility, wear resistance, corrosion resistance, etc. The main distinguishing feature of HEAs from traditional alloys is that they have a high mixing entropy, which significantly affects their structure and properties [1-3].

It was found that the structures of high-entropy alloys could differ significantly from each other. There are high-entropy alloys with a structure based on solid solutions, mixtures of intermetallic phases, amorphous phases as well as alloys with a complex multiphase structure [1-7]. Due to their high hardness and wear resistance, resistance to ionizing radiation, antibacterial properties, and corrosion resistance, high-entropy alloys are promising materials for various fields of technology [8-17].

Recently, it has been proposed in the literature to consider as HEAs only equimolar alloys, the structure of which contains only simple solid solutions with BCC and FCC crystal lattices. For other alloys with high entropy but with non-equimolar component content or more complex phase composition, which also contains ordered solid solutions and intermetallic compounds, it was proposed to introduce new terms, namely: multi-principal element alloys (MPEAs), compositional complex alloys, or complex concentrated alloys (CCAs) [18]. However, at present, these names are not yet common. Studies show that non-equimolar alloys significantly expand the possibilities of improving the characteristics of HEAs, as they can consist of several phases with fundamentally different properties, such as plastic FCC phase and solid and brittle intermetallic phase. Substances that combine the properties of several different types of materials are of considerable scientific interest [19, 20]. A striking example of a non-equimolar HEA is the so-called high-entropy steel or high-entropy alloy, the main component of which is iron [21].

Casting methods are usually used as methods for producing high - entropy alloys.

However, it should be noted that the formation of the structure of solid solution doped with many elements should complicate the casting process, in particular, we can assume a heterogeneous distribution of elements as well as the presence of significant internal stresses in the ingot. There is an obvious need to increase the number of melts to increase the homogeneity of the chemical composition and control the cooling rate during crystallization.

One of the widespread methods of improving the physical, chemical, mechanical and other properties of metals and alloys is hardening from the liquid state (HLS) [22]. The development of HLS methods has led to a growing interest in materials with thermodynamically nonequilibrium structures worldwide. In these methods, the cooling rate of the melt reaches values over 10^6 K/s and therefore a wide range of metastable structural states is formed in the alloys, including nanocrystalline and solid amorphous states with unique sets of properties. Due to this, HLS is a hopeful method for obtaining high-entropy alloys with improved physical characteristics.

In this work, we investigate the influence of the rapid quenching from melt on the phase composition and improvement of some physical properties, in particular, the microhardness and corrosion resistance of non-equiatomic high-entropy alloys of Fe–Cr–Cu–Ni–Mn–Si and Fe–Co–Cu–Ni–Mn–Si systems.

2. Experimental details

The as-cast samples of Fe–Cr–Cu–Ni–Mn–Si and Fe–Co–Cu–Ni–Mn–Si non-equiatomic high-entropy alloys with nominal compositions presented in Table 1 were prepared with a Tamman high-temperature electric furnace in the argon gas flow using a copper mold.

Table 1

Nominal chemical compositions of $Fe_5CrCuNiMnSi$ and $Fe_5CoCuNiMnSi$ high-entropy alloys

	Fe	Cr	Co	Cu	Ni	Mn	Si
Composition of $Fe_5CrCuNiMnSi$, at.%	50	10	0	10	10	10	10
Composition of $Fe_5CoCuNiMnSi$, at.%	50	0	10	10	10	10	10

The mass losses during ingot preparation did not exceed 1% and the average rate of cooling was ~10^2 K/s. The as-cast ingot was thereafter remelted, and the nanostructured films were obtained from the melt by splat quenching (SQ) technique. A technique for splat quenching used in the present work consisted of rapid cooling of melt drops upon their collision with the internal surface of a rapidly rotating hollow cylinder of copper. The cooling rate was estimated following the methodology proposed in [22]. We used the expression

$$V = \frac{\alpha \vartheta}{c \rho \delta} \qquad (1)$$

where c is the heat capacity of the film, ρ is the film density, α is the coefficient of heat transfer, ϑ is the excess temperature of the film and δ is its thickness. Taking into account the thickness of fabricated splat quenched films, i.e., ~40 μm, the estimated rate of cooling was ~10^6 K/s. The X-ray diffraction analysis (XRD) was carried out using a DRON-2.0 diffractometer with monochromatized CuK_α radiation. The diffraction patterns were processed using QualX2 software. The microhardness was examined using a tester PMT-3 at a load of 50 g.

For electrochemical research, the PI-50-1 potentiostat with PR-8 programmer and three-electrode cell were used. Samples of the studied alloys were used as working electrodes. The auxiliary electrode was a platinum plate, and the reference electrode was a silver chloride half-element connected to a cell through a Luggin capillary filled with a

working solution. The studies were performed in 5% (0.9 mol/l) neutral sodium chloride solution. The pH of the solutions was controlled using an ionomer EV-74. The solutions were not mixed during the experiments, their temperature was maintained within 20 ± 2 °C. Methods of electrochemical and corrosion studies are described in detail in previous works [24].

The surface condition of samples during corrosion tests was monitored visually and using a NEOPHOT-21 microscope.

3. Results and discussion

In our previous works [24, 25], the parameters commonly used to predict the phase composition of high-entropy alloys were described. They include entropy of mixing of components ΔS_{mix}, enthalpy of mixing ΔH_{mix}, thermodynamic parameter Ω, topological parameter δ, which characterizes the difference in atomic radii of alloy components and concentration of valence (*s* + *d*) electrons per one atom (*VEC*).

According to [1-3], alloys, for which the value of the $\Delta S_{mix} \geq 11$ J/(mol·K), can be considered as high-entropy. In the structure of HEAs, for which $\Omega \geq 1.1$ and $\delta \leq 6.6\%$, instead of complex intermetallic compounds and amorphous phases, solid replacement solutions are formed (simple and ordered) [1-3]. In this case, the formation of unordered solid solutions should be expected if the value of the mixing enthalpy lies in the range of -15 kJ/mol $< \Delta H_{mix} < 5$ kJ/mol and $\delta \leq 4.6\%$ [1-3]. The type of crystal lattice for solid solutions formed in the structure of HEA is associated with the concentration of valence electrons. The following ratios were proposed [1-3]: formation of a solid solution with an FCC type lattice should be expected at *VEC* > 8, with a BCC type lattice – at *VEC* < 6.87, and at 6.87 < *VEC* < 8 one should expect the formation of two-phase solid solutions based on BCC and FCC lattices. All the above-mentioned parameters for the studied HEAs of Fe–Cr–Cu–Ni–Mn–Si and Fe–Co–Cu–Ni–Mn–Si systems were calculated and given in Table 1.

Table 1

Values of ΔH_{mix}, ΔS_{mix}, δ, VEC and Ω for $Fe_5CrCuNiMnSi$ and $Fe_5CoCuNiMnSi$ high-entropy alloys

Alloy	ΔH_{mix}, kJ/mol	ΔS_{mix}, J/(mol·K)	δ, %	*VEC*	Ω
$Fe_5CrCuNiMnSi$	–10.36	12.45	3.48	7.8	2.11
$Fe_5CoCuNiMnSi$	–10.64	12.45	3.45	8.1	2.01

Based on the values of these parameters, it can be assumed that in the $Fe_5CoCuNiMnSi$ alloy the formation of a solid solution of the FCC type should take place, and in $Fe_5CrCuNiMnSi$ – (BCC type + FCC type).

The study of X-ray diffraction patterns of as-cast HEAs (Fig. 1) revealed that in the structure of the studied high-entropy alloys the basis is composed of disordered solid solutions with crystal lattices of the FCC type. However, while the $Fe_5CoCuNiMnSi$ alloy is single-phase, the phase composition of the $Fe_5CrCuNiMnSi$ alloy is more complex. It contains two FCC phases together with the BCC phase (Table 2), which confirms the results of theoretical prediction of the phase composition of the studied HEAs. Since BCC phases are usually characterized by higher hardness and brittleness compared to softer and more plastic FCC phases, the resulting average microhardness of the $Fe_5CrCuNiMnSi$ alloy should be higher than that of $Fe_5CoCuNiMnSi$.

Since the samples of the investigated alloys in the splat quenched state did not differ from the as-cast ones in terms of the chemical composition, the results of the phase composition prediction should be fair in this case as well. However, the study of XRD patterns of both SQ alloys (Fig. 2) revealed only disordered solid solutions with lattices of the FCC-type (Table 2).

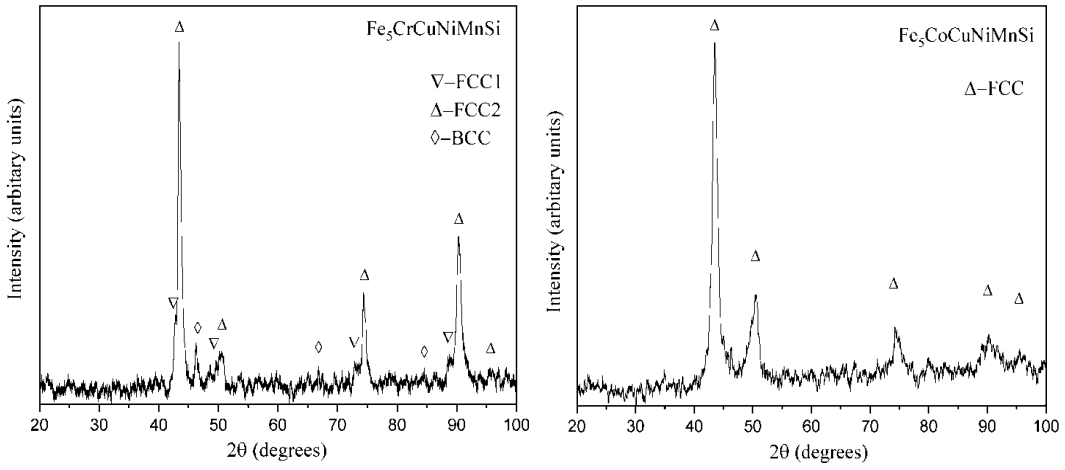

a b

Fig. 1. XRD patterns of casted $Fe_5CrCuNiMnSi$ (a) and $Fe_5CoCuNiMnSi$ (b) high-entropy alloys.

Table 2

The phase composition and crystal lattice parameters of as-cast and splat quenched $Fe_5CrCuNiMnSi$ and $Fe_5CoCuNiMnSi$ high-entropy alloys

Alloy	Phase composition
As-cast $Fe_5CoCuNiMnSi$	FCC (a = 0.361nm)
As-cast $Fe_5CrCuNiMnSi$	FCC1 (a = 0.3656 nm) + FCC2 (a = 0.3607 nm) + BCC (a = 0.281 nm)
SQ $Fe_5CoCuNiMnSi$	FCC (a = 0.3601nm)
SQ $Fe_5CrCuNiMnSi$	FCC (a = 0.3615 nm)

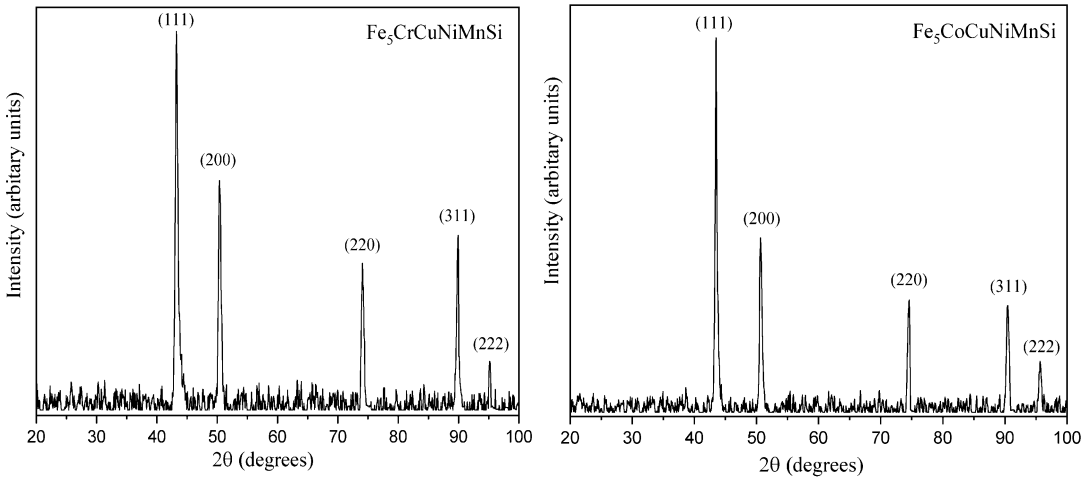

a b

Fig. 2. XRD patterns of $Fe_5CrCuNiMnSi$ (a) and $Fe_5CoCuNiMnSi$ (b) spalt-quenched high-entropy alloy films.

That is, the forecast calculations regarding the phase composition of the studied HEAs came true only partially. The reason why the phase composition of the SQ samples of $Fe_5CrCuNiMnSi$ alloy does not correspond to the predicted one and differs from the phase composition of as-cast samples is obviously that in the thermodynamically nonequilibrium structure of the SQ film only crystalline nuclei of the main FCC phase have time to form and grow. The second FCC and BCC phases, which obviously have a lower crystallization temperature, do not have time to form. This is indicated by the fact

that even in an as-cast alloy of $Fe_5CrCuNiMnSi$ obtained in much more equilibrium conditions with a low cooling rate (10^2 K/s), their content is insignificant, which follows from the low intensities of the corresponding diffraction maxima (Fig. 1). Thus, it can be argued that the estimated prediction of the phase composition of HEAs does not allow to describe the phase composition of alloys obtained from the melt by splat quenching method fully.

Fig. 3 shows the polarization dependences obtained for the studied as-cast alloys in 5% NaCl solution at pH = 6.9. Based on the obtained dependencies, it can be stated that for the $Fe_5CoCuNiMnSi$ alloy the area of electrochemical inertness is narrower and is in the range from –1.0 V to –0.3 V. For the $Fe_5CrCuNiMnSi$ alloy the area of electrochemical inertness is in the range from –1.0 V to –0.1 V, i.e.it expanded in the anode direction by 0.2 V. This can be explained by the replacement of cobalt in the alloy composition with chromium, which upon oxidation forms compounds capable of passivating the surface. The corrosion process in neutral saline for both alloys occurs with oxygen depolarization. Under such conditions, the determining stage is usually the diffusion of oxygen to the surface.

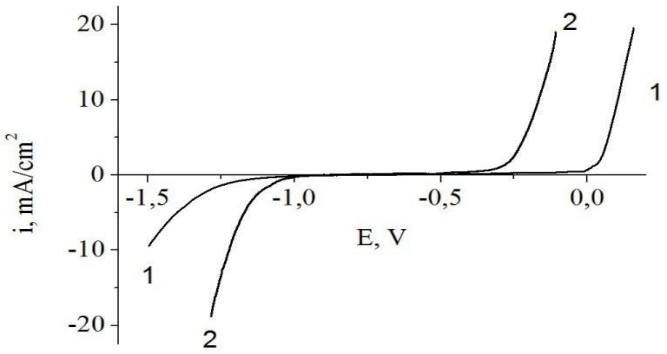

Fig. 3. Polarization dependences obtained for cast alloys $Fe_5CrCuNiMnSi$ (1) and $Fe_5CoCuNiMnSi$ (2) in 5% NaCl solution.

Fig. 4 shows the areas of polarization dependences near the values of stationary potentials, constructed in semi-logarithmic coordinates, from which the densities of corrosion currents i_{corr} were determined. The logarithm of this quantity corresponds to the point of intersection of tangents to the two branches of the graph. It was found that for the $Fe_5CoCuNiMnSi$ alloy the i_{corr} is equal to 0.18 mA/cm^2 and it is significantly higher than the i_{corr} for the $Fe_5CrCuNiMnSi$ alloy (0.07 mA/cm^2).

Similar polarization measurements were performed for SQ samples. The obtained results are shown in Fig. 5. As can be seen, the area of electrochemical stability for the alloy $Fe_5CoCuNiMnSi$ is in the range from –1.0 V to –0.3 V, and for the alloy $Fe_5CrCuNiMnSi$ from 1.0 V to –0.1 V. That is, for an alloy containing chromium, this area expanded to the range of more positive potentials and by the same amount as in the case of cast alloys. The values of corrosion current densities for SQ samples were calculated by processing the results of polarization measurements in semi-logarithmic coordinates with lg *i*, *E* dependences (Fig. 6). The calculated values of i_{corr} are given in Table 3.

Model corrosion tests of samples were performed by their complete immersion in NaCl solution at a temperature of 20 ± 2 °C with periodic monitoring of the surface

condition after 1, 2, 4 and 8 days from the beginning of the experiment. The results of corrosion tests show that the alloy $Fe_5CoCuNiMnSi$, both in as-cast and SQ state, is not corrosion-resistant. After a day of testing, corrosion products are formed on its surface, which does not have protective properties. $Fe_5CrCuNiMnSi$ alloy samples behave inertly and only films of corrosion products appear on their surface, which is visualized as variability colors.

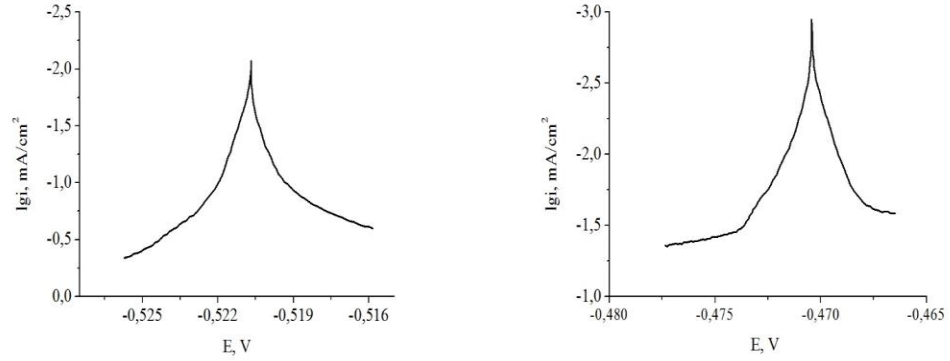

Fig. 4. lg *i*, E - dependences obtained for cast alloys $Fe_5CoCuNiMnSi$ (a) and $Fe_5CrCuNiMnSi$ i (b) in 5% NaCl solution; pH = 6.9; *V* = 1 mV/s.

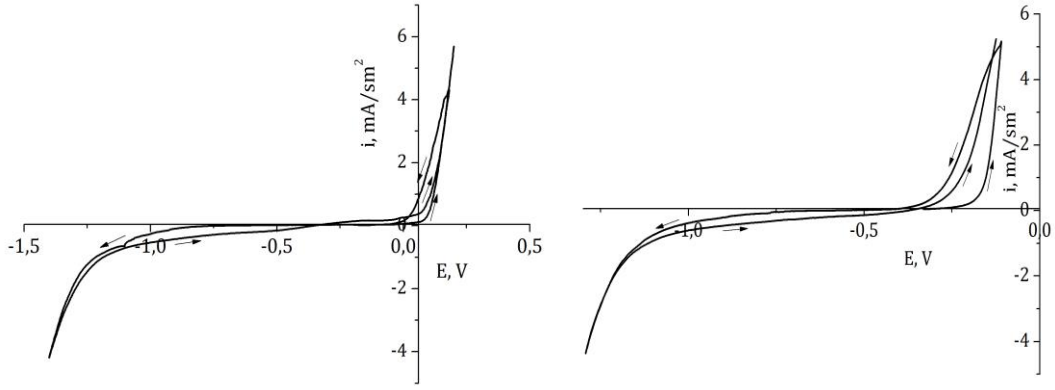

Fig. 5. Polarization dependences obtained for spalt-quenched $Fe_5CrCuNiMnSi$ (a) and $Fe_5CoCuNiMnSi$ (б) alloys in 5% NaCl solution.

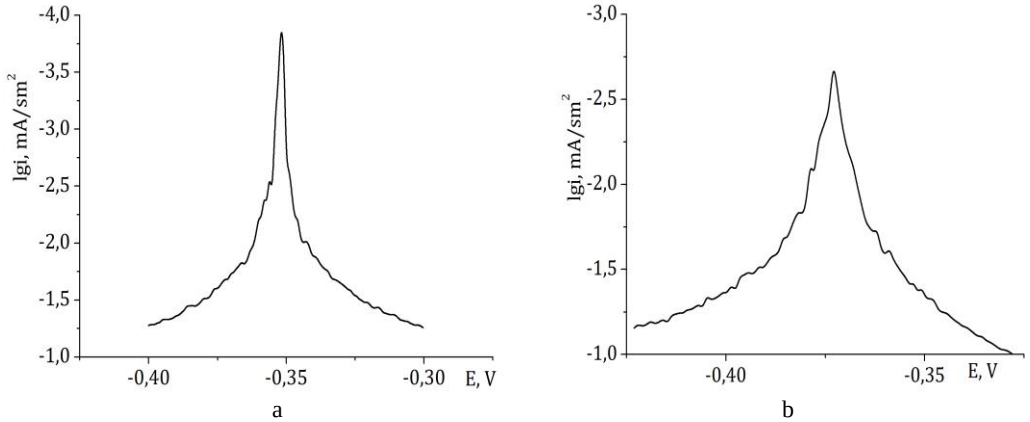

Fig 6. lg *i*, *E* - dependences obtained for spalt-quenched $Fe_5CoCuNiMnSi$ (a) and $Fe_5CrCuNiMnSi$ (b) alloys in 5% NaCl solution.

Table 3

Values of i_{corr} (mA/sm^2) of as-cast and spalt-quenched $Fe_5CrCuNiMnSi$ and $Fe_5CoCuNiMnSi$ alloys

Alloy	As-cast	SQ
$Fe_5CrCuNiMnSi$	0,07	0,03
$Fe_5CoCuNiMnSi$	0,18	0,07

4. Conclusions

It is established that structure of the studied non-equiatomic high-entropy alloys $Fe_5CrCuNiMnSi$ and $Fe_5CoCuNiMnSi$ in the as-casted state is formed by disordered solid solutions with crystal lattices of the FCC type. However, the phase composition of the $Fe_5CrCuNiMnSi$ alloy is more complex and contains two FCC phases together with the BCC phase. The splat-quenched samples are disordered solid solutions based on a cubic structure with lattices of the FCC type. The phase composition and parameters of the crystal lattices of the investigated alloys are determined. It is shown that the theoretical prediction of the phase composition of HEAs does not allow to describe the phase composition of the alloys fully.

According to the results of model corrosion tests conducted in neutral 5% NaCl solution for 1 to 8 days, it was found that the $Fe_5CoCuNiMnSi$ alloy, both in as-cast and SQ state, is not corrosion-resistant. The corrosion products formed on its surface do not have protective properties. It is determined that the samples of $Fe_5CrCuNiMnSi$ alloy behave inertly in corrosion tests. Only thin films of corrosion products appear on their surface in the form of variability colors.

Thus, the application of the method of quenching from the liquid state to obtain high-entropy chromium-containing alloys allows us to obtain a material with sufficiently high characteristics of corrosion resistance. In this case, the studied high-entropy Fe-based alloys in comparison with traditional wind farms are characterized by a relatively low content of Co and Cr, which significantly increase the cost of alloys. Taking into account that SQ samples are usually characterized by improved physical and mechanical characteristics in comparison with the samples obtained by casting, the studied splat-quenched HEAs are promising for practical applications.

References

1. High entropy alloys. Innovations, advances, and applications / Eds. T.S. Srivatsan, M. Gupta. – Boca Raton : CRC Press, 2020. – 758 p.

2. High-entropy alloys. 2nd edition / B.S. Murty, J.W. Yeh, S. Ranganathan, P.P. Bhattacharjee. – Elsevier Science Publishing Co Inc, 2019. – 363 p.

3. High-entropy alloys. Fundamentals and Applications/ Eds. M. C. Gao, J.–W. Yeh, P. K. Liaw, Y. Zhang. – Springer International Publishing, 2016. – 516 p.

4. **Dong, Y.** Microstructure and mechanical properties of AlCoxCrFeNi3-x eutectic high-entropy-alloy system / Y. Dong, Z. Yao, X. Huang, F. Du, C. Li, A. Chen, F. Wu, Y. Cheng, Z. Zhang // Journal of Alloys and Compounds. – 2020. – Vol. 823. – P. 153886.

5. **Kim, Y.K.** Superior temperature-dependent mechanical properties and deformation behavior of equiatomic CoCrFeMnNi high-entropy alloy additively manufactured by selective laser melting / Y.K. Kim, S. Yang, K.A. Lee // Scientific Reports. – 2020. –Vol. 10, No. 1. – P. 1 – 14.

6. **Gadelmeier, C.** Temperature dependent solid solution strengthening in the high entropy alloy CrMnFeCoNi in single crystalline state / C. Gadelmeier, S. Haas, T. Lienig, A. Manzoni, M. Feuerbacher, U. Glatzel // Metals. – 2020. – Vol. 10, No. 11. – P. 1412.

7. **Kushnerov, O.I.** Structure and properties of nanostructured metallic glass of the Fe–B–Co–Nb–Ni–Si high-entropy alloy system / O.I. Kushnerov, V.F. Bashev, S.I. Ryabtsev // Springer Proceedings in Physics, 2021. – P. 557 – 567.

8. **Abdelghafar, K.A.** Evaluation of microstructural and corrosion resistance of as-cast Cu45Mn25Al15Fe5Cr5Ni5 high entropy alloy / K.A. Abdelghafar, M.M. Ibrahim, M.A. Shoeib, M.A. Waly // Materials Research Express. – 2020. – Vol. 7, No. 1. – P. 016579.

9. **Zhou, E.** A novel Cu-bearing high-entropy alloy with significant antibacterial behavior against corrosive marine biofilms / E. Zhou, D. Qiao, Y. Yang, D. Xu, Y. Lu, J. Wang, J. A. Smith, H. Li, H. Zhao, P. K. Liaw, F. Wang // Journal of Materials Science & Technology. – 2020. – Vol. 46. – P. 201 – 210.

10. **Xiang, C.** Design of single-phase high-entropy alloys composed of low thermal neutron absorption cross-section elements for nuclear power plant application / C. Xiang, E.-H. Han, Z. M. Zhang [et al.] // Intermetallics. – 2019. –Vol. 104. – P. 143 – 153.

11. **Patel, D.** Radiation damage tolerance of a novel metastable refractory high entropy alloy V2.5Cr1.2WMoCo0.04 / D. Patel, M.D. Richardson, B. Jim [et al.] // Journal of Nuclear Materials. –2020. –Vol. 531. –P. 152005.

12. **Chen, Y.H.** On the bio-corrosion and biocompatibility of TiTaNb medium entropy alloy films / Y.H. Chen, W.S. Chuang, J.C. Huang [et al.] // Applied Surface Science. –2020. –Vol. 508. –P. 145307.

13. **Perumal, G.** Enhanced biocorrosion resistance and cellular response of a dual-phase high entropy alloy through reduced elemental heterogeneity / G. Perumal, H.S. Grewal, M. Pole [et al.] // ACS Applied Bio Materials. – 2020. –Vol. 3, No. 2. – P. 1233 – 1244.

14. **Firstov, G.S.** High entropy shape memory alloys / G.S. Firstov, T.A. Kosorukova, Y.N. Koval, V.V. Odnosum // Materials Today: Proceedings. – 2015. – Vol. 2. – P. S499 – S503.

15. **Li, Y.** New FeNiCrMo(P, C, B) high-entropy bulk metallic glasses with unusual thermal stability and corrosion resistance / Y. Li, S. Wang, X. Wang [et al.] // Journal of Materials Science & Technology. – 2020. – Vol. 43. – P. 32 – 39.

16. **Lu, J.** Y/Hf-doped AlCoCrFeNi high-entropy alloy with ultra-oxidation and spallation resistance / J. Lu, Y. Chen, H. Zhang [et al.] // Corrosion Science. – 2020.– Vol. 166. – P. 108426.

17. **Coimbrão, D.D.** Corrosion properties of amorphous, partially, and fully crystallized Fe68Cr8Mo4Nb4B16 alloy / D.D. Coimbrão, G. Zepon, G.Y. Koga [et al.] // Journal of Alloys and Compounds. – 2020. – Vol. 826. – P. 154123.

18. **Miracle, D.B.** A critical review of high entropy alloys and related concepts / D.B. Miracle, O.N. Senkov // Acta Materialia. – 2017. – Vol. 122. – P. 448 – 511.

19. **Dudnik, E.F.** Higher order ferroic properties of TGS monocrystals / E.F. Dudnik, A.I. Kushnerev, V.M. Duda // Materials Research Innovations. – 1999. – Vol. 2, No. 5. – P. 309 – 311.

20. **Dudnik, E.F.** Second-order ferroic properties of a Pb5Ge3O11 uniaxial ferroelectric / E.F. Dudnik, V.M. Duda, A.I. Kushnerov // Physics of the Solid State. – 2001. – Vol. 43, No. 12. – P. 2280 – 2283.

21. **Raabe, D.** From high-entropy alloys to high-entropy steels / D. Raabe, C.C. Tasan, H. Springer, M. Bausch // Steel Research International. – 2015. – Vol. 86, No. 10. – P. 1127 – 1138.

22. **Miroshnichenko, I.S.** Quenching from the Liquid State / I.S. Miroshnichenko. – Metallurgiya, Moscow, 1982. – 168 p. [in Russian].

23. **Polonskyy, V.A.** Structure and corrosion-electrochemical properties of Fe-based cast high-entropy alloys/ V.A. Polonskyy, V.F. Bashev, O.I. Kushnerov // Journal of Chemistry and Technologies. – 2020. – Vol. 28, No. 2. – P. 177 – 185.

24. **Kushnerov, O.I.** Structure and physical properties of cast and splat-quenched CoCr0.8Cu0.64FeNi high entropy alloy / O.I. Kushnerov, V.F. Bashev // East European Journal of Physics. – 2021. – No. 3. –P. 43 – 48.